RSC Advances

ROYAL SOCIETY OF CHEMISTRY

www.rsc.org/advances

Cite this: DOI: 10.1039/c0xx00000x

www.rsc.org/xxxxxx

ARTICLE TYPE

$Bi_2Sn_2O_7$-TiO_2 nanocomposites for enhancing visible light photocatalytic activity

Yonglei Xing, Wenxiu Que*, Xiaobin Liu, H. M. Asif Javed, Zuoli He, Yucheng He, Ting Zhou

Received (in XXX, XXX) Xth XXXXXXXXX 20XX, Accepted Xth XXXXXXXXX 20XX

DOI: 10.1039/b000000x

$Bi_2Sn_2O_7$-TiO_2 nanocomposites with different ratios of $Bi_2Sn_2O_7$ (BSO) and TiO_2 were prepared by combining a facile co-precipitation method with an aid of template. X-ray diffraction, X-ray photoelectron spectroscopy and transmission electron microscopy were employed to characterize the physicochemical properties of the as-prepared nanocomposites. The band gap energies of the nanocomposites were established by diffuse reflectance UV-Vis spectra. The specific surface area and average pore diameter of the nanoparticles were measured by N_2 adsorption-desorption isotherm. Photocatalytic degradation of rhodamine B dye molecules was also investigated in the visible region so as to explore the photocatalytic activity of the as-prepared nanocomposites. Results showed that the 10BSO-TiO_2 nanocomposites have a remarkably enhanced photocatalytic performance as compared with other samples including anatase TiO_2. It was also found that all BSO modified TiO_2 samples have wider band gap energy than pure BSO sample, but showed a higher photocatalytic activity than pure BSO sample due to the photosensitization mechanism of the dye molecules.

1. Introduction

Over the past few decades, semiconductor photocatalysts have been extensively studied due to environment accountability and energy conversion.[1-3] Among various oxide semiconductor photocatalysts, titanium dioxide (TiO_2), which emerges as one of the most fascinating materials, has succeeded in capturing attention of physical chemists, physicists and material scientists to explore its distinctive semiconducting and photocatalytic properties. [4-7] Especially, it has been used in photocatalysts, dye-sensitized solar cells, gas sensors and many other applications. [8-15] However, the relative wide band gap (3.2 eV for anatase TiO_2) has seriously restricted its applications. Therefore, many technologies have been developed to make TiO_2 respond to visible light for efficient utilization of solar energy. [16-20]

Due to the presence of titanium interstitials, TiO_2 behaves as an n-type semiconductor. [21, 22] Hence the doping of various metal and nonmetal ions, which include Ag, Cd, Mo, Nd, Sr, Cl, C, N, S and F, into TiO_2 by substituting for lattice Ti atoms or oxygen atoms has been studied to improve its visible light absorption. [23-30] However, the shortcomings of the doping might result in irregular structures and lattice defects, which mainly act as the recombination centres and thus shorten the lifetime of the electron-hole pairs. [31] Actually, modification of TiO_2 by metal oxidation has been proposed to be one of the efficient methods to visualize TiO_2 photocatalysts.

Recently, a great deal of effort has been devoted to developing photocatalysts containing bismuth element due to their high activities for environmental applications, [32] such as Bi_2WO_6, [33] $Bi_2O_2CO_3$ [34] and $Bi_2Sn_2O_7$. [35] Murcia-López et al [36] synthesized Bi_2WO_6-TiO_2 photocatalyst, which showed a band gap of 2.9 eV and had high photoactivity for Rhodamine B degradation under sunlight illumination. $Bi_2Sn_2O_7$ with the pyrochlore structure is known as a novel semiconducting material, which can respond to visible light due to its narrow band gap. [37] It is reported that $Bi_2Sn_2O_7$ has a complicated structure with three different polymorphs α (monoclinic), β (face-centered cubic), and γ (cubic), thus leading to different optical properties. With the contribution of s-orbital to valence band and conduction band, $Bi_2Sn_2O_7$ has the potential to increase its catalytic efficiency by producing electron and hole with high mobility. [38] Among the Bismuth-based pyrochlores, bismuth titanium compounds have served as potential photocatalysts.[39, 40] Here, we reported the synthesis and photocatalytic activities of the $Bi_2Sn_2O_7$-TiO_2 nanocomposites with different $Bi_2Sn_2O_7$ compositions by combining a co-precipitation method with an aid of template. Results indicated that the adding of $Bi_2Sn_2O_7$ can enhance the photocatalytic activity for the degradation of Rhodamin remarkably and the corresponding photocatalytic mechanism was also discussed.

2. Experimental

2.1 Synthesis of $Bi_2Sn_2O_7$-TiO_2 nanocomposite

All the reactants were commercially purchased and used without any further purification. $Bi_2Sn_2O_7$ was prepared by a similarly previous method as reported in Ref. [38]. A typical synthesis of $Bi_2Sn_2O_7$ compound was as follows: $Bi(NO_3)_3{\cdot}5H_2O$, $K_2SnO_3{\cdot}3H_2O$, and HNO_3 were used as the starting reactants, and stoichiometric amounts of the $Bi(NO_3)_3{\cdot}5H_2O$ and $K_2SnO_3{\cdot}3H_2O$ reactants were dissolved in minimum amount of dilute HNO_3

(1:10 v/v). The mixed hydroxides were then precipitated by adding liquid $NH_3 \cdot H_2O$ till the solution became alkaline. The precipitates were filtered, washed thoroughly with water and dried at 400-500 °C. Finally, the dried powders were pressed into pellets and heated at 750 °C for 6 h.

$Bi_2Sn_2O_7$ (BSO) modified TiO_2 nanoparticles were prepared by a similar method as reported in Ref. [31] except for some modification. Briefly, $Ti(OBu)_4$ was added dropwise into a mixture of absolute ethanol (20 mL) and water (10 mL) to obtain a turbid solution under a magnetic stirring for 2h at room temperature. After stirring for 5 h, an appropriate amount of BSO was added into the solution and 0.5 g of PEG-4000 was also added as templates. The suspension was further stirred for another 5 h, and then heated directly by an alcohol burner while being stirred by a glass rod so that the solvent can be evaporated. Finally, the dried powder was collected, ground and activated at 450 °C for 2.5 h. The as-obtained samples were designated according to the atomic percentage of BSO, including 1BSO-TiO_2, 5BSO-TiO_2, 10BSO-TiO_2 and 15BSO-TiO_2.

2.2 Characterization

Crystalline properties of the as-prepared samples were characterized by powder X-ray diffractometry (D/max-2200, Rigaku, Japan) using Cu Kα radiation. Composition identification of the products were performed by using X-ray photoelectron spectroscopy (XPS) from Axis Ultra, Kratos (UK) using monochromatic Al Kα radiation (150 W, 15 KV, 1486.6 eV) under a vacuum pressure of 10^{-9} Torr. All the binding energies of the products were referenced to the C1s peak (284.80 eV) from hydrocarbons adsorbed on the surface of the samples. Optical absorbance of the samples was measured by diffuse reflectance UV-Vis (DRUV-vis) spectra from a JASCO Model V-570 UV/VIS/NIR spectrometer equipped with a diffuse reflectance accessory in the region from 200 nm to 800 nm. Transmission electron microscopy (TEM, JEM-2010) was employed to observe the morphological properties of the as-prepared products, which were dispersed in ethanol ultrasonically and then a drop of liquid was dropped on a thin amorphous carbon film supported by the copper grid. The specific surface area and average pore diameter of the nanoparticles were measured by N_2 adsorption-desorption isotherm from an Automated Surface area and Porosity Analyser.

2.3 Measurement of photocatalytic activity

Photocatalytic activity of the as-prepared products was evaluated by measuring the photodegradation of Rhodamine B (RhB) in aqueous medium under visible light irradiation. The concentrations of initial RhB solution and the as-prepared products were 10 mg/L and 1 mg/mL, respectively. The photoreaction was conducted in a BL-GHX-V multifunctional photochemical reactor by using a 500W Xe arc lamp with a 420 nm cutoff filter as the irradiation source to imitate the natural light. In order to attain adsorption-desorption equilibrium between the RhB and the photocatalyst, the suspension was stirred in the dark for 1 h. The concentration of the RhB was estimated by measuring the absorption of the resulted solution at 554 nm from JASCO V-570 UV/VIS/NIR spectrometer.

3. Results and discussion

3.1 Crystalline property

As seen in experimental, BSO was synthesized by the co-precipitation reaction of $Bi(NO_3)_3 \cdot 5H_2O$ and $K_2SnO_3 \cdot 3H_2O$ in acidic solution and then heated at 750 °C. It should be mentioned here that there is a little difference between the present preparation process and the method as reported in Refs. [38, 41], that is, TiO_2 was here prepared in the addition of BSO to form the BSO-TiO_2 nanocomposites. Simultaneously, BSO was also induced by the hydrolytic process. Thus, all the reactions in the experiment may occur as follows:

$$SnO_3^{2-} + 3H_2O \rightarrow Sn(OH)_6^{2-} \leftrightarrow Sn(OH)_4 + 2OH^- \quad (1)$$

$$Bi^{3+} + 3OH^- \rightarrow Bi(OH)_3 \quad (2)$$

$$2Sn(OH)_4 + 2Bi(OH)_3 \rightarrow Bi_2Sn_2O_7 + 7H_2O \quad (3)$$

$$Ti(OC_4H_9)_4 + H_2O \leftrightarrow (C_4H_9O)_3TiOH + C_4H_9OH \quad (4)$$

$$(C_4H_9O)_3TiOH + H_2O \leftrightarrow (C_4H_9O)_2Ti(OH)_2 + C_4H_9OH \quad (5)$$

$$(C_4H_9O)_2Ti(OH)_2 + H_2O \leftrightarrow C_4H_9OTi(OH)_3 + C_4H_9OH \quad (6)$$

$$C_4H_9OTi(OH)_3 + H_2O \leftrightarrow Ti(OH)_4 + C_4H_9OH \quad (7)$$

$$Ti(OH)_4 \rightarrow TiO_2 + 2H_2O \quad (8)$$

Figure 1 shows the XRD patterns of the pure TiO_2 and the BSO modified TiO_2 samples. It can be seen that there are no any other peaks except for the diffraction peaks of BSO and TiO_2, indicating that the as-prepared samples under present conditions have a high purity. It is also observed that the pure $Bi_2Sn_2O_7$ sample synthesized at 750 °C can be indexed to the pyrochlore family along with the splitting peak at 33.5° in α-form and some extra small superstructure peaks between 35° and 45°, indicating the presence of less symmetric α- or β-polymorphs of BSO as reported in the literature (JCPDS No. 34-1203). [42] The diffraction peaks of the pure TiO_2 sample at 25.26, 36.94, 48.05, 53.89, 55.06 and 62.68° correspond to the reflections from the (101), (004), (200), (105), (211) and (204) crystal planes of anatase TiO_2, respectively, which also confirm a good crystalline nature of TiO_2 (JCPDS No. 21-1272). For those modified TiO_2 samples with different BSO compositions, most of the peaks perfectly match with those of the pure TiO_2 and BSO, indicating the as-obtained products have a coexistence of TiO_2 and BSO. As compared with the pure TiO_2 sample, the diffraction peaks of the modified samples are comparatively broad, suggesting that nanocrystals are formed in these modified samples. [43] In addition, the diffraction peaks of the modified samples become broader as the BSO content increases, and the peak intensity of the BSO phase in the modified samples becomes more intense with an increase of the addition amount of BSO from 1 at% to 15 at%. Furthermore, the peak splitting of the modified samples can be clearly observed at 25.26° towards a higher angle, which probably originates from the (444) facet of the diffraction peak of the BSO phase, thus leading to a similar d-spacing value to the (101) plane of anatase TiO_2. These results indicate that the close interaction between BSO and TiO_2 phase structure significantly exists. Especially, some minor peaks between 39° and 45° disappear in all the modified samples as compared to the BSO sample, which further provide an evidence of the interaction between the two components of BSO and TiO_2.

Based on the XRD results, the crystal size of the nanocomposite was calculated by the Scherrer equation. Result as presented in Table 1 indicates that the crystal size increases with the increase of the BSO component, which suggests that the presence of BSO can promote the crystal growth of TiO_2 during the calcination process due to the heterojunction interface between TiO_2 and BSO nanocrystals. The variation of the crystal size of the nanocomposite with the BSO component further demonstrates the interaction between TiO_2 and BSO.

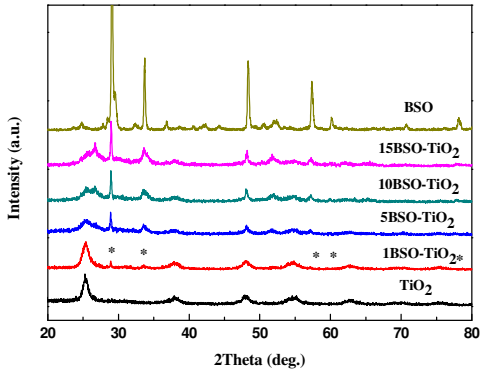

Fig. 1 XRD patterns of TiO_2, BSO and BSO modified TiO_2 samples

Table 1 Crystallite size (nm) of the samples.

Samples				
TiO_2	1BSO-TiO_2	5BSO-TiO_2	10BSO-TiO_2	15BSO-TiO_2
8.2	8.8	17.0	55.2	51.7

3.2 Transmission electron microscopy observation

TEM micrographs of the TiO_2, BSO and 10BSO-TiO_2 samples are shown in Fig. 2. It can be observed from Figure 2(c) that the BSO nanoparticles can be embedded into the TiO_2 nanoparticles to form the nanocomposite with bigger crystallite size, which is in good agreement with the result of XRD. Therefore, it can be concluded that the 10BSO-TiO_2 sample consists of distinguished irregular nanoparticles with different sizes between 5 to 20 nm, that is, the sample is composed of the BSO and TiO_2 nanoparticles with diverse sizes. Furthermore, the HRTEM was also used to verify the presence of both BSO and TiO_2 phase composition. Actually, well crystalline characteristic of the sample can be also confirmed from the HRTEM observation as shown in Figure 2(b). The lattice fringes with an interplanar spacing 0.352 nm and 0.266 nm correspond to the (101) plane of TiO_2 and (800) plane of BSO, respectively. The HRTEM results are in good agreement with the data from XRD. It can be concluded from above results that the BSO-TiO_2 nanocrystal heterojunction is actually formed in the nanocomposites.

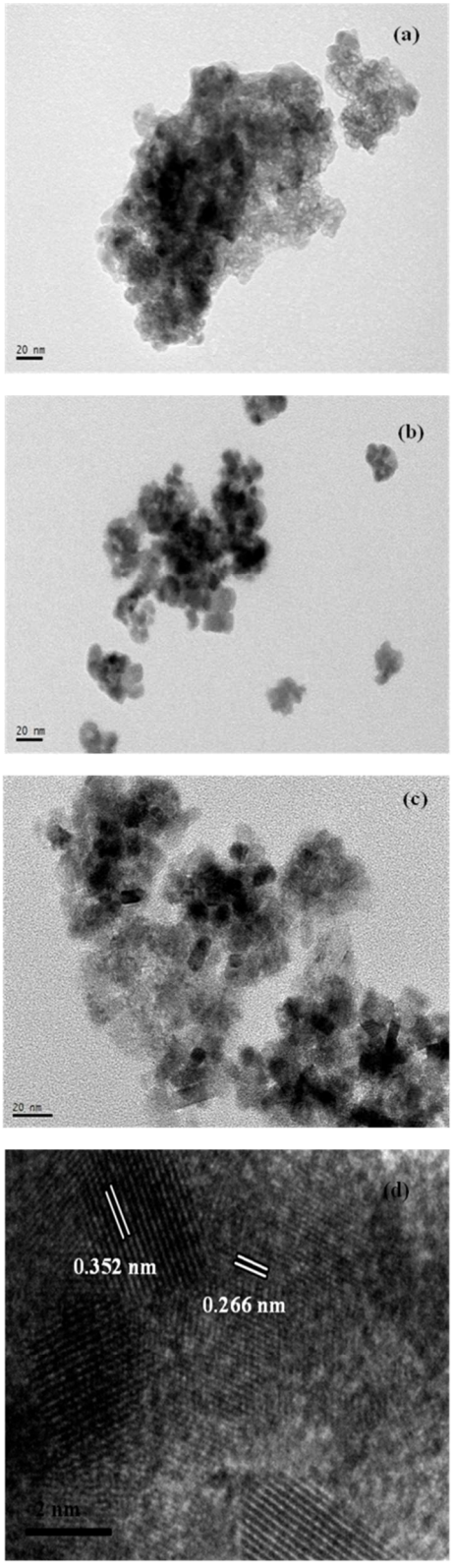

Fig. 2 TEM images of TiO_2 (a), BSO (b) and 10BSO-TiO_2 sample (c), and HRTEM image of 10BSO-TiO_2 sample (d)

3.3 XPS study

In order to study the chemical composition and oxidation state of the as-prepared samples, XPS spectrum of the 10BSO-TiO_2 sample was performed. Figure 3a shows the measured result,

where the C is mainly ascribed to an adventitious hydrocarbon from XPS system itself. Figure 3b shows the XPS spectrum of the Ti 2p region, indicating the splitting photo electrons from the Ti 2p 1/2 spin-orbital and Ti 2p 3/2 spin-orbital locate at binding energies of 464.4 and 458.5 eV respectively, which correspond to that of the Ti^{4+} oxidation state. The peak located at 529.9 eV is assigned to O 1s as shown in Fig 3c, which is in agreement with that as reported in Ref. [44]. It can be seen that the O 1s peak is broad and complicated, which is probably related to the non-equivalence of the surface oxygen ions. This simple peak is different from the splitting peak existed in the doped-TiO_2 nanomaterials and it might result from the overlapping contribution of the oxide ions, which are probably related to the O^{2-} of bismuth oxide and titanium oxide. The spectrum as shown in Fig. 3d exhibits the binding energies of 486.4 and 494.8 eV, which originate from Sn 3d 5/2 and Sn 3d 3/2 of stannum compounds. Moreover, the binding energy of Sn 3d 5/2 is consistent with the literature value of Sn^{4+} in BSO as reported in Ref [32]. Figure 3e is XPS spectrum of Bi 4f, two symmetric peaks at 164.5 eV and 159.2 eV are assigned to Bi $4f_{5/2}$ orbital and Bi $4f_{7/2}$ orbital, which correspond to Bi^{4+} and Bi^{3+}, respectively. [32] It can be concluded that the XPS results as shown in Fig. 3 present a further evidence for the biphase composition of the as-prepared nanocomposite.

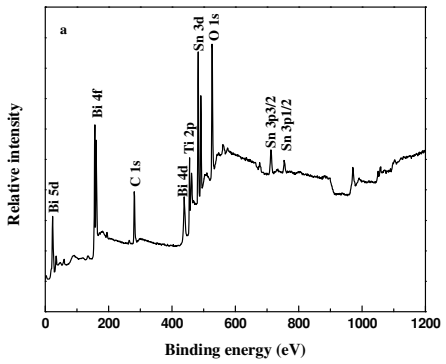

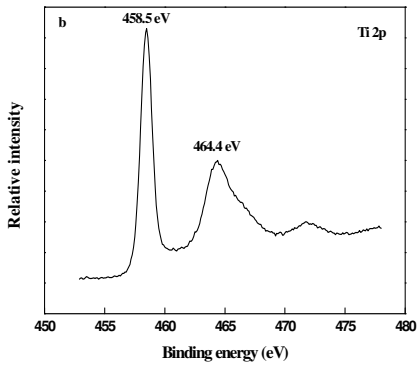

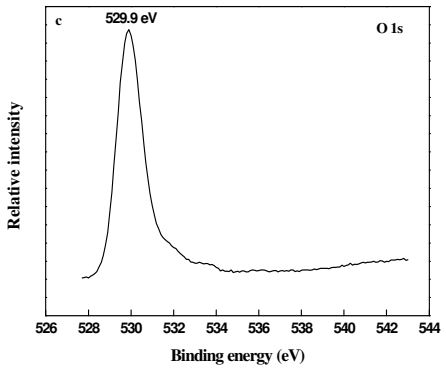

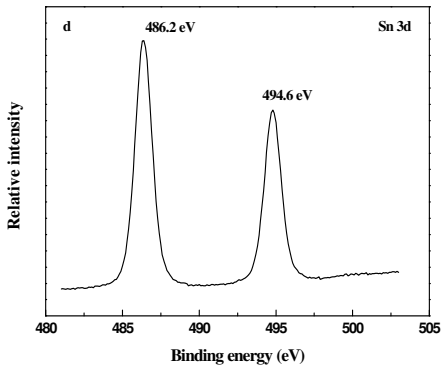

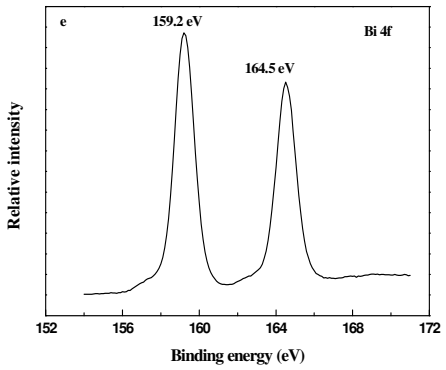

Fig. 3 (a) XPS survey spectrum of 10BSO-TiO_2 sample, (b) Spectrum of Ti 2p, (c) Spectrum of O 1s, (d) Spectrum of Sn 3d, (e) Spectrum of Bi 4f

3.4 Optical properties

Room temperature optical absorption spectra of the pure TiO_2 and the BSO-TiO_2 nanocomposites in the wavelength range between 200 nm and 800 nm are shown in Fig 4a. It can be seen that the pristine TiO_2 displays no absorption for visible light due to wide energy gap of 3.05 eV, which is 0.15 eV lower than the reported value, [32] due to trace amount of carbon element from the template into TiO_2 during the calcination process. However, the BSO-TiO_2 nanocomposites show a significant spectral response in the visible region and the absorbance of these samples increases with the increase of the BSO content from 1 to 15 at%.

The relationship between the absorption coefficient and the

band gap of semiconductor can be expressed as follows based on Tauc's formula. [31]

$$F(R)\, hv = B\,(hv - Eg)^n \quad (9)$$

Where A is the absorption coefficient, hv is the photon energy, B is a constant and n is a value that depends on the nature of the electron transition, which is responsible for the absorption (n=1/2 for direct transition and n=2 for indirect transition). Here, the n value for all samples is determined to be 2 according to the described method.[45]

The band gaps of all samples are presented in Fig. 4 (b). The band gap energy of TiO_2 is high and only absorbs UV light, but BSO is able to absorb visible light. Therefore, it is easy to understand that the as-prepared BSO-TiO_2 nanocomposites can successively absorb visible light. Actually, as can be seen from Fig.4a, the absorption edges of all BSO modified TiO_2 samples shift towards a longer wavelength region.

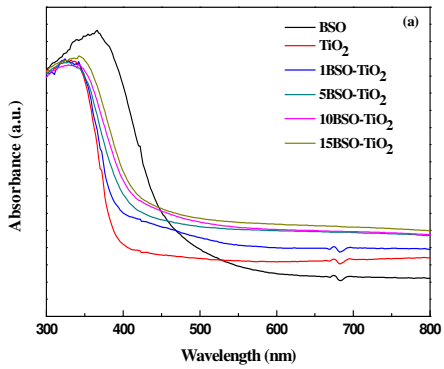

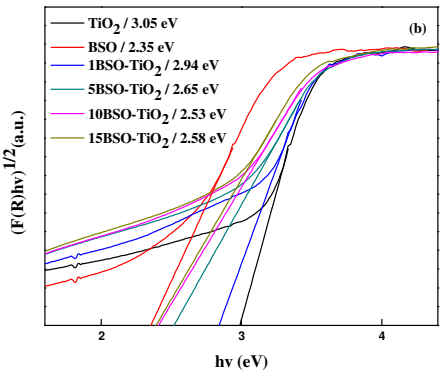

Fig. 4 Optical absorption spectra (a) and estimated band gap energies (b) of the TiO_2 and BSO modified TiO_2 samples.

3.5 BET analysis

The specific surface area and porosity of the TiO_2 and 15BSO-TiO_2 sample were investigated by using nitrogen adsorption and desorption isotherm. The isotherms as shown in Figure 5a can be categorized as type IV with a distinct hysteresis loop, exhibiting a mesoporous structure. The BET specific surface area of TiO_2 is 69.6 $m^2 \cdot g^{-1}$ and its pore diameter is about 3.72 nm. However, the 15BSO-TiO_2 composite has a little higher surface area (71.2 $m^2 \cdot g^{-1}$) and larger pore diameter (5.83 nm), which is beneficial for the interaction between TiO_2 and BSO nanoparticles.

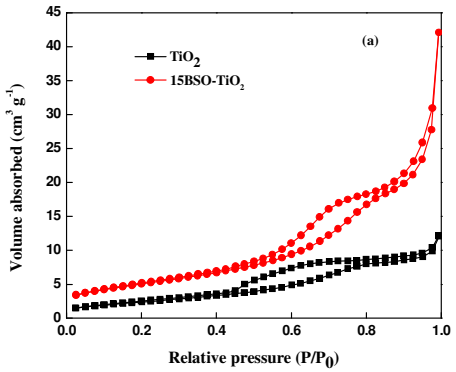

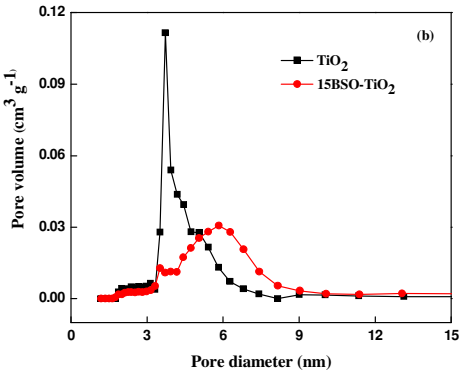

Fig. 5 (a) Nitrogen adsorption/desorption isotherms and (b) BJH (Barrett-Joyner-Halenda) pore size distribution of TiO_2 and 15BSO-TiO_2 sample

3.6 Photocatalytic performances and mechanism under visible light irradiation.

Photocatalytic activities of the pure TiO_2 and BSO-TiO_2 nanocomposite photocatalyst under the simulative sunlight irradiation were examined with RhB, which has an initial concentration of 2×10^{-5} mol/L C_0, as the test contaminant. Figure 6 shows the as-obtained results. The blank test of the pure TiO_2 photocatalyst exhibits low photodegradation efficiency and thus the concentration of RhB decreases slowly under the visible light irradiation, it is due to that very small account of carbon element from surfactant is doped into TiO_2. However, the concentration of RhB decreases sharply under the exposure in the presence of the BSO-TiO_2 nanocomposite. In addition, it is also noted that the degradation efficiency of RhB increases with the increase of the BSO content in the nanocomposite owing to the increase of the number of active sites, which are helpful for the photocatalytic activity of the BSO-TO_2 nanocomposite. [44] As shown in Figure 6, about 80% of RhB can be photodegraded by the catalysis of the 10BSO-TiO_2 nanocomposite within 120 minutes. Especially, amongst all of the photocatalysts including P25, the 10BSO-TiO_2 nanocomposite photocatalyst shows the highest photocatalytic activity.

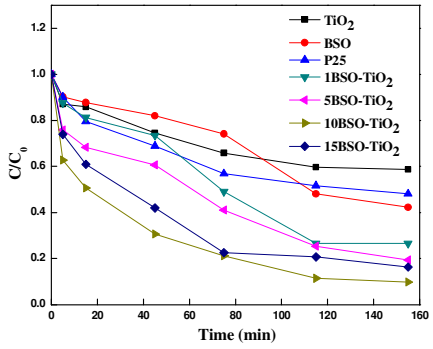

Fig. 6 Temporal courses of the decrease in the RhB concentration with visible-light irradiation time

An interesting observation of the gradual shift in λ_{max} of the RhB dye solution with an addition of the 10BSO-TiO_2 nanocomposite as a function of irradiation time is shown in Figure 7a. It can be seen that the λ_{max} shifts to the blue side due to the de-ethylation process of RhB giving rhodamine as shown in Fig. 8, thus, it can absorb light with shorter wavelength and lead to an increasing of blue shift as the duration of irradiation increases, which is in better accordance with the result given by Sayed, et al. [33, 38] In addition, it can be seen from Fig. 7b that there is not any blue shift to be observed for the λ_{max} of the RhB dye solution during the irradiation due to the different degradation mechanism of the de-ethylation process. That is to say, there is a competition between de-ethylation and degradation during the irradiation. Moreover, it will produce N,N,N'-triethylated rhodamine (λ_{max}= 539 nm), N,N'-diethylated rhodamine (λ_{max}=523nm), N-ethylated rhodamine (λ_{max}=510nm), and rhodamine (λ_{max}=498nm) during the de-ethylation process. [46] Hence it can be concluded from above results that the degradation of the chromophore ring is the predominant pathway in the presence of the pure BSO as compared to the de-ethylation step, while the opposite occurs for the case of the BSO-TiO_2 nanocomposite during the irradiation of visible light. [47] These results indicate that the pure BSO has lower photocatalytic activity than the 10BSO-TiO_2 nanocomposite in the de-ethylation process due to the the quick recombination of the photogenerated electron-hole pairs, that is to say, the heterojunction structure between BSO and TiO_2 is beneficial for the separation of the photogenerated charge carriers.

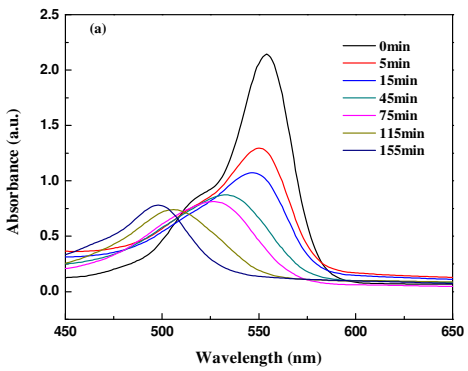

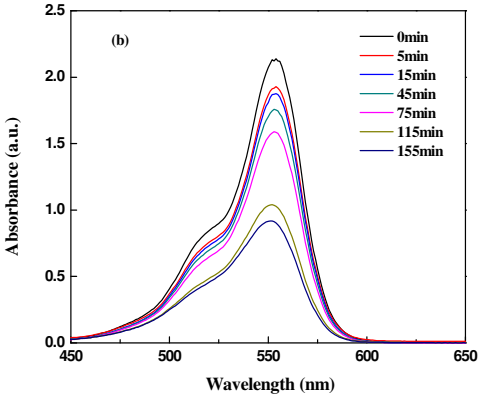

Fig. 7 Representative degradation profiles of RhB in the presentence of (a) 10BSO-TiO_2 sample and (b) pure BSO sample

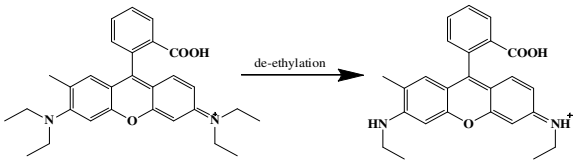

Fig. 8 De-ethylation process of Rhodamine B

One plausible explanation for the degradation mechanism of the RhB solution could be the different band gap of the photocatalysts. The rhodamine B molecules belong to intensely colored conjugation species and can absorb the visible light strongly. Thus, the dye molecule is excited to an appropriate excited state by visible light and then the electrons transfer from the dye molecules to the conduction band of the photocatalysts. [48] This electron can then react with the pre-adsorbed oxygen to form oxidizing species resulting in the photooxidiation of dyes. This photooxidiation process, as shown in Scheme 1, is called photosensitization, which has been widely used in dye-sensitized solar cells. [47,49] In the case for the only BSO solution, however, although the self-photosensitization process of the dye still exists in the process of the photodegradation, the semiconductors to absorb the photon with larger energy than the band gap of the material play the main role in generating holes and electrons in valence and conduction band, respectively. Since the band gap of the pure BSO is narrower than that of the BSO-TiO_2 nanocomposite, hence two mechanisms including de-ethylation and degradation occur in the photodegradation process of RhB for the nanocomposite photocatalyst under the visible light irradiation.

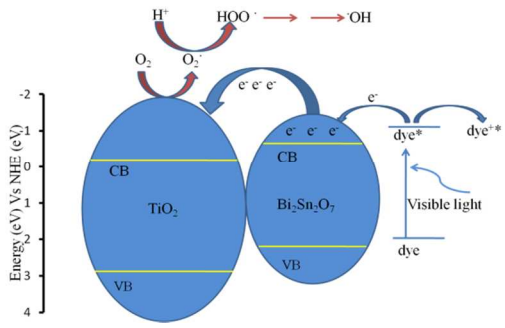

Scheme 1 Mechanism of photodegradation under visible light irradiation

4. Conclusions

The BSO-TiO_2 nanocomposites with heterojunction structure have been successfully synthesized by combining the co-precipitation route with the aid of template. The optical properties of the as-synthesized BSO-TiO_2 nanocomposites have been significantly improved due to the introduction of the BSO. As compared with TiO_2, the absorption edges of the BSO-TiO_2 nanocomposites shift to a longer wavelength region. Enhanced photocatalytic activities for rhodamine B degradation of the BSO-TiO_2 nanocomposite photocatalyst have been confirmed, in which the 10BSO-TiO_2 nanocomposite sample shows the highest photocatalytic activity. Under the visible light irradiation, two different degradation pathways are suggested during the degradation process of the rhodamine B molecules due to the difference in band gap. It can be concluded that the as-prepared BSO-TiO_2 nanocomposites with heterojunction structure will give a new insight to the photocatalytic activity of TiO_2.

Acknowledgements

This work was supported by the Research Fund for the Doctoral Program of Higher Education of China under grant 20120201130004, partially the National Natural Science Foundation of China Major Research Plan on Nanomanufacturing under Grant No. 91323303, the National Natural Science Foundation of China under Grant No. 61078058, and the 111 Project of China (B14040). The SEM and TEM works were done at International Center for Dielectric Research, Xi'an Jiaotong University, Xi'an, China. The authors also thank Ms. Dai and Mr Ma for their help in using SEM and TEM.

Notes and References

*Electronic Materials Research Laboratory, International Center for Dielectric Research, Key Laboratory of the Ministry of Education, School of Electronic and Information Engineering, Xi'an Jiaotong University, Xi'an 710049, Shaanxi, P.R.China. *Tel.: +86-29-82668679; Fax: +86-29-82668794. Email address: wxque@mail.xjtu.edu.cn*

1 J. Wang, D. N. Tafen, J. P. Lewis and Z. L. Hong, *J. Am. Chem. Soc.,* 2009, **131**, 12290.
2 N. J. Bell, Y. H. Ng, A. J. Du, H. Coster, S. C. Smith and R. Amal, *J. Phys. Chem. C,* 2011, **115**, 6004.
3 X. B. Chen and S. S. Mao, *Chem. Rev.,* 2007, **107**, 2891.
4 N. L. Yang, Y. Y. Liu, H. Wen, Z. Y. Tang, H. J. Zhao, Y. L. Li and D. Wang, *ACS Nano.*, 2013, **7**, 1504.
5 D. Jassby, J. F. Budarz and M. Wiesner, *Environ. Sci. Technol*., 2012, **46**, 6934.
6 S. W. Liu, J. G. Yu and M. Jaroniec, *J. Am. Chem. Soc*., 2010, **132**, 11914.
7 F. Dong, H. Q. Wang and Z. B. Wu, *J. Phys. Chem. C* 2009, **113**, 16717.
8 S. Kitano, N. Murakami, T. Ohno, Y. Mitani, Y. Nosaka, H. Asakura, K. Teramura, T. Tanaka, H. Tada, K. Hashimoto and H. Kominami, *J. Phys. Chem. C* 2013, **117**, 11008.
9 Y. Cong, J. L. Zhang, F. Chen, M. Anpo and D. N. He, J. Phys. Chem. C 2007, **111**, 10618.
10 J. L. Zhang, Y. M. Wu, M. Y. Xing, S. A. K. Leghari and S. Sajjad, Energy Environ. Sci., 2010, **3**, 715.
11 K. Chandiran , P. Comte , R. Humphry-Baker , F. Kessler , C. Y. Yi, M. K. Nazeeruddin and M.Grätzel, Adv. Funct. Mater., 2013, **23**, 2775.
12 H. J. Son, C. Prasittichai, J. E. Mondloch, L. L. Luo, J. S. Wu, D. W. Kim, O. K. Farha and Joseph T. Hupp, J. Am. Chem. Soc. 2013, **135**, 11529.
13 W. Zeng, T. M. Liu and Z. C. Wang, J. Mater. Chem., 2012, **22**, 3544.
14 R. Daghrir, P. Drogui and D. Robert. Ind. Eng. Chem. Res., 2013, **52**, 3581.
15 S. Ho-Kimura , S. J. A. Moniz , A. D. Handoko and J. W. Tang, J. Mater. Chem. A, 2014, **2**, 3948.
16 X. D. Yan, C. W. Zou, X. D. Gao and W. Gao, J. Mater. Chem., 2012, **22**, 5629.
17 S. Tojo, T. Tachikawa, M. Fujitsuka and T. Majima, J. Phys. Chem. C 2008, **112**, 14948.
18 H. Kato and A. Kudo, J. Phys. Chem. B 2002, **106**, 5029.
19 F. Gao, X. Y. Chen, K. B. Yin, S. Dong, Z. F. Ren, F. Yuan, T. Yu, Z. G. Zou and J. M. Liu, Adv. Mater., 2007, **19**, 2889.
20 L. J. Zhang and M. X. Wan, J. Phys. Chem. B 2003, **107**, 6748
21 C. Chen, W. M. Cai, M. C. Long, B. X Zhou, Y. H. Wu, D. Y. Wu and Y. J. Feng, ACS Nano., 2010, **4**, 6425.
22 A. Wisitsoraat, A. Tuantranont, E. Comini, G. Sberveglieri and W. Wlodarski, Thin Solid Films, 2009, **517**, 2775.
23 Y. C. Yang, J. W. Wen, J. H. Wei, R. Xiong, J. Shi and C. X. Pan, ACS Appl. Mater. Interaces, 2013, **5**, 6201.
24 G. S. Li, D. Q. Zhang and J. C. Yu, Environ. Sci. Technol., 2009, **43**, 7079.
25 J. Zhang, C. X. Pan, P. F. Fang, J. H. Wei and R. Xiong, ACS Appl. Mater. Interfaces, 2010, **2**, 1173.
26 X. Y. Wu, S. Yin, Q. Dong, C. S. Guo, T. Kimura, J. I. Matsushita and T. Sato. J. Phys. Chem. C 2013, **117**, 8345.
27 L. Kumaresan, M. Mahalakshmi, M. Palanichamy and V. Murugesan, Ind. Eng. Chem. Res., 2010, **49**, 1480.
28 F. Dong, S. Guo, H. Q. Wang, X. F. Li and Z. B. Wu, J. Phys. Chem. C 2011, **115**, 13285.
29 K. S. Yang, Y. Dai, B. B. Huang and M. H. Whangbo, Chem. Mater., 2008, **20**, 6528.
30 X. B. Chen and C. Burda, J. Am. Chem. Soc., 2008, **130**, 5018.
31 S. Martha, K. H. Reddy and K. M. Parida, J. Mater. Chem. A, 2014, **2**, 3621.
32 W. C. Xu, G. Y. Zhou, J. Z. Fang, Z, Liu, Y. F. Chen and C. P. Cen, International Journal of Photoenergy, 2013, **2013**, 1 .
33 T. Saison, P. Gras, N. Chemin, C. Chanéac, O. Durupthy, V. Brezová, C. Colbeau-Justin and J. P. Jolivet, J. Phys. Chem. C 2013, **117**, 22656.
34 F. Dong, Y. J. Sun, M. Fu, W. K. Ho, S. C. Lee and Z. B. Wu, Langmuir, 2012, **28**, 766.
35 J. J. Wu, F. Q. Huang, X. J. Lü, P. Chen, D. Y. Wan and F. F. Xu, J. Mater. Chem., 2011, **21**, 3872.
36 S. Murcia-López, M. C. Hidalgo and J. A. Navío, Photochemistry and Photobiology, 2013, **89**, 832.
37 A. Walsh and G. W. Watson, Chem. Mater. 2007, **19**, 5158.
38 F. N. Sayed, V. Grover, B. P. Mandal and A. K. Tyagi, J. Phys. Chem. C 2013, **117**, 10929.
39 A. Salamat, A. L. Hector, P. F. McMillan and C. Ritter. Inorg. Chem., 2011, **50**, 11905.
40 S. J. Henderson, O. Shebanova, A. L. Hector, P. F. McMillan and M. T. Weller, Chem. Mater., 2007, **19**, 1712.
41 W. J. Wang, J. H. Bi, L, Wu, X. Z. Fu, Photocatalyst. Nanotechnology. 2008, **19**, 505705.
42 R. D. Shannon, J. D. Bierlein, J. L. Gillson, G. A. Jones, A. W. Sleight, J. Phys. Chem. Solids, 1980, **41**, 117.
43 K. M. Parida, K. H. Reddy, S. Martha, D. P. Das and N. Biswal, Int. J. Hydrogen Energy, 2010, **35**, 12161.
44 M. Ge, Y. F. Li, L. Liu, Z. Zhou and W. Chen, J. Phys. Chem. C 2011, **115**, 5220.
45 J. Luan, Z. Zou, M. Lu, G. Luan and Y. Chen, Res. Chem. Intermed., 2006, **32**, 31.
46 D. W. Hwang, J. S. Lee, W. Li and S. H. Oh, J. Phys. Chem. B 2003, **107**, 4963.
47 T. Wu, G. Liu, J. Zhao, H. Hidaka and N. Serpone, J. Phys. Chem. B 1998, **102**, 5845.

48 J. He, J. Zhao, T. Shen, H. Hidaka and N. Serpone, J. Phys. Chem. B 1997, **101**, 9027.
49 M. Grätzel, Journal of Photochemistry and Photobiology C: Photochemistry Reviews, 2003, **4**, 145-153.